RSC Advances

PAPER

View Article Online
View Journal | View Issue

Cite this: *RSC Adv.*, 2022, **12**, 3243

A soft intelligent dressing with pH and temperature sensors for early detection of wound infection†

Zhiyang Zhang,‡[ab] Rui Su,‡[bc] Fei Han,‡[d] Zhiqiang Zheng,[b] Yuan Liu,[b] Xiaomeng Zhou,[d] Qingsong Li,[d] Xinyun Zhai,[e] Jun Wu,[f] Xiaohua Pan,[g] Haobo Pan,[b] Peizhi Guo,[c] Zhaoyang Li,[a] Zhiyuan Liu *[d] and Xiaoli Zhao *[b]

Received 16th November 2021
Accepted 16th January 2022

DOI: 10.1039/d1ra08375a

rsc.li/rsc-advances

Wound infection is a common clinical problem. Traditional detection methods can not provide infection early warning information in time. With the development of flexible electronics, flexible wearable devices have been widely used in the field of intelligent monitoring. Here, we describe the development of a soft wound infection monitoring system with pH sensors and temperature sensors. The measurement range of pH was 4–10, the fitting accuracy was 99.8%, and the response time was less than 6 s. The temperature sensor array showed good accuracy and short response times in the range of 30 °C to 40 °C. A series of *in vitro* tests and the use of a rat model of *Staphylococcus aureus* infection confirmed that this flexible detection system can monitor the pH and temperature changes occurring in the early stage of infection, which provides an effective reference for clinical application.

1. Introduction

Skin injuries caused by trauma, surgery, or diabetes have a high prevalence and cause enormous medical and financial burdens.[1,2] Bacterial infection is a potentially serious complication and can significantly delay healing, while also possibly leading to a pronounced systemic inflammatory response syndrome.[3] Chronic wounds, which affect approximately 1–2% of the global population, are highly susceptible to infection. Foot ulcers, in particular, are now the leading cause of non-traumatic morbidity. Therefore, prevention and management of infections is important for patients with nonhealing or traumatic injuries; in particular, early diagnosis of bacterial infections is considered highly important for halting the progression of associated diseases.[4]

Early detection of pathogenic infections is often difficult before clinical signs and symptoms appear.[5] Currently, clinicians mainly rely on conventional culture-based approaches using wound swabs to identify infective bacterial species. Final results of these tests usually take 3–5 days, so this approach does not provide timely guidance.[6] Dressings are usually needed to cover the wound to protect wounds from pathogenic infections and to provide a humid environment that accelerates healing. The dressings are changed every 2–3 days, during which the wound condition was difficult to directly observe. Therefore, a pressing need exists to develop dressings that can monitor wound conditions and predict infections. The basic requirement for this smart dressing is the conformability to the wound, because a wound's surface is always cambered, and the smart dressing needs to firstly adhere well to it for detecting desired signals. Many phenomena are caused by infection, such as changes in metabolites, protein signals, pH, and temperature. Specific biomarker of bacteria has relatively high specificity, but infection is often caused by multiple bacteria and complicated factors. Previous studies have shown that pH and temperature, as common physiological parameters, are closely related to the changes of wound.[7,8] For skin pH, normal skin has an acidic pH, ranging between 4 and 6. Since body's internal environment maintains a neutral, the pH will rise when a wound is formed. Once infection occurs, the proliferation of microorganisms will induce the pH to rise to even slightly alkaline. At the same time, the temperature of the wound will also rise due to the inflammatory reaction and the relaxation of

[a]*School of Materials Science and Engineering, Tianjin Key Laboratory of Composite and Functional Materials, Tianjin University, Tianjin 300350, PR China*

[b]*Research Center for Human Tissue and Organs Degeneration, Institute of Biomedicine and Biotechnology, Shenzhen Institutes of Advanced Technology Chinese Academy of Sciences, Shenzhen 518055, PR China. E-mail: zhaoxltju@gmail.com*

[c]*Institute of Materials for Energy and Environment, State Key Laboratory of Bio-fibers and Eco-textiles, School of Materials Science and Engineering, Qingdao University, Qingdao 266071, PR China*

[d]*Neural Engineering Center, Shenzhen Institute of Advanced Technology, Chinese Academy of Sciences, Shenzhen 518055, PR China. E-mail: zy.liu1@siat.ac.cn*

[e]*Center for Rare Earth and Inorganic Functional Materials, School of Materials Science and Engineering, National Institute for Advanced Materials, Nankai University, Tianjin 300350, PR China*

[f]*Shenzhen Key Laboratory for Innovative Technology in Orthopaedic Trauma, The University of Hong Kong-Shenzhen Hospital, Shenzhen 518053, PR China*

[g]*Southern Medical University, Shenzhen Bao'an People's Hospital, Dept Orthoped & Traumatol, Shenzhen 518101, PR China*

† Electronic supplementary information (ESI) available. See DOI: 10.1039/d1ra08375a

‡ These authors contributed equally to this work.

its own blood vessels, and the infection will aggravate this trend.[9–11] Therefore, the changes of wound pH and temperature are widely studied parameters to determine the wound state. They are the simplest and most effective parameters to design the sensor. Previous studies have used optical signals to monitor skin surface pH and temperature, but the closed environment of the wound limits the optical signal, so the monitoring method based on electrical signals is more suitable for the wound environment.[12–15] A single monitoring method is easy to be disturbed by the external environment. For example, the temperature change of the environment will affect the human body temperature to a certain extent. Therefore, we monitor two physiological parameters at the same time to obtain more accurate monitoring data.

Previously, based on the developed flexible electronic, advanced dressings were developed to monitor the state of acute and chronic wounds.[16–18] Some of these dressings use commercial temperature sensor chips, combined with intelligent bandages, to monitor and treat infected wounds on demand, thereby confirming the possibility of combining hard electronic devices with flexible circuits.[19,20] At the same time, new chemical sensors have been developed that can be integrated with flexible circuits, and electrochemical methods are now widely used.[21,22] Chemical sensors, such as pH sensors based on potentiometry and glucose sensors based on cyclic voltammetry, can output signals through electrical signals, thereby providing convenient data transmission for monitoring infection processes.[23–26] In reported studies, polyethylene terephthalate (PET) and polyimide (PI) serve as flexible substrates, but lacking softness limits their adhesion to wounds.[21,27] Therefore, the substrate needs a stretchable material such as polydimethylsiloxane (PDMS), polyurethane, styrene ethylene butylene styrene (SEBS). The stretchability of the material can ensure that the sensor can always have a good relatively static contact with the wound when the wound deforms. SEBS shows the best stretchability and softness, and has been used as wearable electronics,[28,29] however, it has not been applied in wound monitoring.

Herein, we propose a new hybrid flexible dressing for early detection of wound infection by employing thin SEBS elastomer film as substrates combined with polyaniline (PANI) based pH sensor and commercial temperature sensor (Fig. 1A). The temperature and pH values can be recorded to grasp the physiological changes of the wound in real-time. PANI, as a good conductive polymer, shows different open circuit potential (OCP) in solutions with different pH values, which is caused by its protonation reaction in acidic solutions. And the pH sensor integrated on SEBS substrate has the characteristics of softness and stretchability. The measurement range was pH 4–10, fitting accuracy was 99.8%, and the response time was less than 6 s. The temperature sensor showed good accuracy and short response times in the range of 30 to 40 °C. Fig. 1B shows both sensors converted information into electrical signals, pH sensor is based on potential, while temperature sensor is based on Negative Temperature Coefficient (NTC). A series of *in vitro* tests and the use of a rat model of *Staphylococcus aureus* infection confirmed that this flexible detection system can monitor the pH and temperature changes occurring in the early stage of infection (Fig. 1C), which provides an effective reference for clinical application.

2. Materials and methods

2.1. Materials

The Ag/AgCl paste was purchased from ALS Co., Ltd. (Japan). Aniline, KCl, HCl, and H_2SO_4 were obtained from the Sinopharm group. SEBS was obtained from Asahi Kasei Chemical Co., Ltd. (Japan). Methylbenzene and phosphate buffered saline (PBS; pH = 7.2–7.4) were obtained from Aladdin. The pH buffer (pH 4–10) was bought from Concord Technology (Tianjin). Temperature sensor chips, polyimide (PI) and the FPCB were purchased from Lichuang (Shenzhen). Deionized water (DI) and Millipore water were used in all experiments. All chemicals were used as received, without any further purification.

2.2. Fabrication of the stretchable substrate with pH sensor

The pH sensor consisted of an Ag/AgCl reference electrode and a polyaniline (PANI) working electrode. The fabrication process involved three main steps. SEBS dissolves in methylbenzene to get solution, the 15% SEBS solution was dropped onto a Si wafer and allowed to air dry to form a polymer film (thickness: 200 μm) for the stretchable circuit. Gold particles were then sputtered onto the SEBS surface with a magnetron sputtering apparatus (TWS-300), and electrodes were formed on the SEBS with a stainless mask. Ultra-thin SEBS film was used for packaging, and it only exposed the position of the corresponding monitoring point and circuit interface. The final pH working electrode was prepared by electrochemical deposition of a PANI solution on a CHI760E electrochemical workstation (CH Instruments Inc., Shanghai). The method of electrochemical deposition is based on previous studies.[30,33] For the reference electrode, Ag/AgCl (10 μL ink) was dropped onto the Au surface within an area of 2 × 2 mm, and a layer of polyvinyl butyral (PVB) containing KCl was covered.[34] The resulting pH sensor was dried at room temperature.

2.3. Preparation of the temperature sensor

The temperature sensor was prepared utilizing a commercial TMP112AIDRLR with a two-wire serial output in a small-sized transistor. The small transistors were soldered onto the FPCB. The temperature measurement was conducted with a designed Debug board and the FPCB. The real-time temperature was displayed on the screen.

2.4. Characterization and measurements by the sensors

The morphologies of the Au, Ag/AgCl, and PANI were studied by field-emission scanning electron microscopy (FESEM, Phenom Pharos). The infrared spectra of the PANI samples were obtained with a VERTEX80 micro-infrared system. The mechanical properties of the material and the electromechanical robustness of the stretchable Au traces were measured with an AG-X Plus universal testing machine (Japan). The sensing performance of the pH sensor, including the pH-OCP curve,

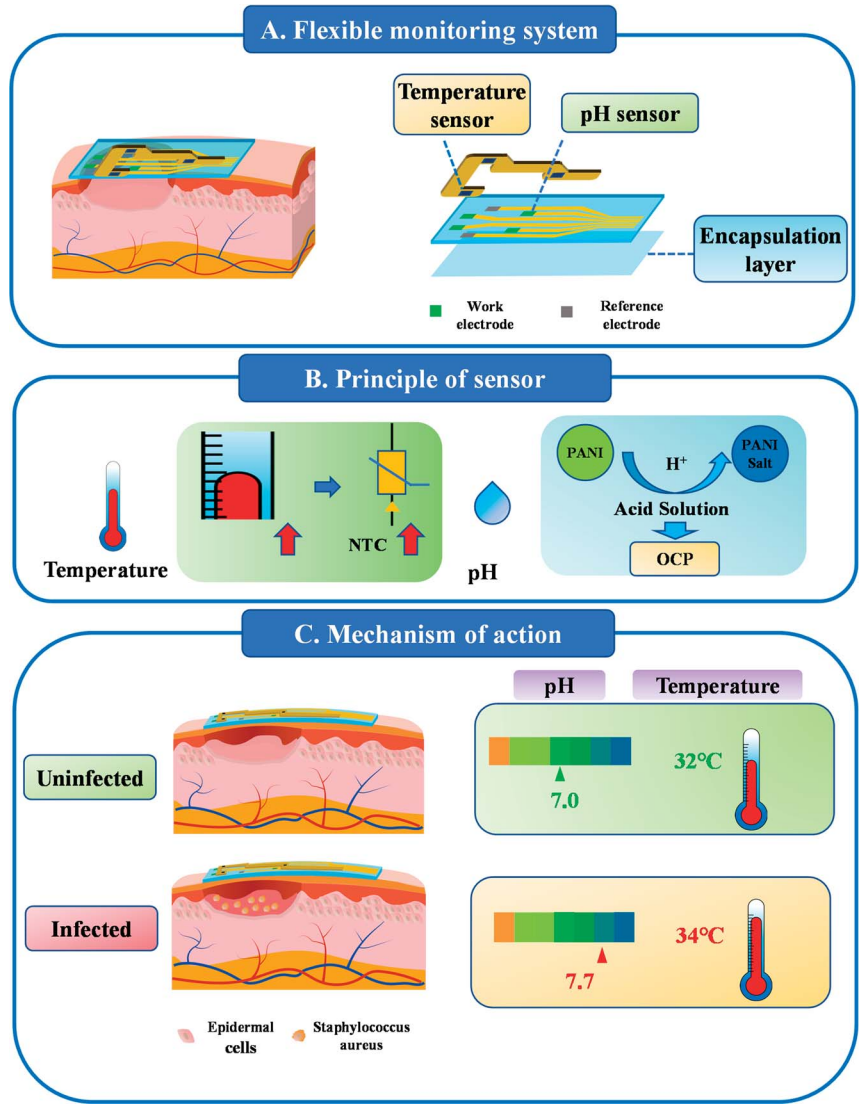

Fig. 1 The flexible wound infection monitoring system with pH sensors and temperature sensors. (A) Structure of flexible wound infection monitoring system. (B) Principle of pH and temperature sensors in transmitting signals into electrical signals. (C) The changes of pH and temperature were monitored during wound infection (OCP: open circuit potential, NTC: negative temperature coefficient, PANI: polyaniline).

response time, and stability, was tested on the electrochemical workstation.

2.5. *In vitro* biocompatibility assessment

Mouse L929 cells were used to study the biocompatibility of the materials used in the pH sensor and temperature sensor by testing cell viability with the CCK-8 assay. L929 cells were cultured in α-minimum essential media (α-MEM, Gibco) supplemented with 10% FBS (Corning) and 1% penicillin/streptomycin (P/S, Invitrogen) in a humidified incubator (5% CO_2) at 37 °C. All materials (SEBS, Au, Ag/AgCl, and PANI) were shaped into circular 5 mm diameter disks. The materials were incubated in fresh culture medium at 37 °C (3 cm^2 mL^{-1}) for 24 h. The cells were seeded into a 96-well plate at a density of 1 × 10^3 cells per well and incubated for 24 h. The cells were then exposed to the different extracts, with extract medium refreshed every other day. Cell viability was assessed using a CCK-8 kit (Beyotime), according to the manufacturer's instructions.

2.6. Wound infection monitoring

Wound infection was evaluated by creating a rat model of wound infection using *S. aureus*. Female Sprague Dawley (SD) rats were purchased from Beijing Charles River Animal Co., Ltd. Ten 6 weeks-old SD rats were used in the animal experiment. All animal experiments conformed to the National Institutes of Health guidelines, and protocols were approved by the committee of Shenzhen Institute of Advanced Technology, CAS.

A cutaneous wound was created on the back of each rat, and the animals were divided into two groups: uninfected and infected. The rats were anesthetized with isoflurane, and the dorsal hair was shaved to expose the skin. After sterilization of the shaved area with 75% alcohol and iodine, a square full-

thickness skin wound (2 cm × 2 cm) was made with scissors. The fascia part of the lower dermis was removed with sterilized forceps, and the fascia was destroyed with scissors. The wounds were washed with saline, blotted with sterile gauze, and then inoculated with *S. aureus* suspension (50 μL, 1×10^9 CFU) to induce the bacterial infection. Rats that received physiological saline instead of bacterial suspension served as controls. The flexible dressing with sensors was placed on the wound sites to monitor the wound status and then covered with transparent 3M dressing. The pH and temperature were monitored at 0, 8, 24, 32, 54, and 78 h.

2.7. Histologic analysis

A biopsy of the wounded tissue was obtained at 8 and 30 h. All samples were fixed in neutral formalin (10%) for 24 h and then washed in running water for 3 h, dehydrated in a graded ethanol series, and embedded in paraffin. Sections (6 μm thick) were cut from each paraffin block and placed on glass slides. The sections were deparaffinized, rehydrated, stained with hematoxylin and eosin (H&E), and viewed by light microscopy.

2.8. Statistical analysis

Data are expressed as mean ± standard deviation (SD). Statistical analysis was performed by two-tailed Student's *t*-tests between two groups or by one-way ANOVA between more than two groups. Asterisks (*) indicate a statistical significance of $p < 0.05$.

3. Results and discussion

3.1. Fabrication and characterization of the pH sensor

A flexible pH sensor was constructed on the modification of a flexible electrode. A sputtering method was used to fabricate a layer of gold electrode array film with a thickness of 100–150 nm on the surface of the SEBS film. The advantage is that both the substrate and the electrode can be made very thin. This means that the process will not affect its softness. The PANI film was prepared by electrochemical deposition on the surface of gold electrode to serve as a working electrode. From the cyclic voltammogram of electrochemical deposition, the redox peak value gradually increases as time goes on, which indicated that PANI has been successfully deposited on the gold electrode (Fig. S2†). The Ag/AgCl reference electrode was prepared by a drop-coating method to form the pH sensor.

FT-IR spectroscopy was used to confirm the successful synthesis of PANI, as shown in Fig. 2A. The prominent peaks of the PANI-based electrode at 1548, 1499, and 806 cm^{-1} corresponded to C=C stretching of the quinoid ring, C=C stretching of the benzenoid ring, C–N stretching of the benzenoid unit, and C–H out-of-plane bending, indicating the successful preparation of polyaniline functional films. The SEM image of the Ag/AgCl reference electrode is shown in Fig. 2B. No cracks or holes were evident, indicating strong adhesion of the Au and Ag/AgCl electrodes. Observation of the interface between PANI and the Au electrodes by SEM revealed an obvious boundary. The flaky micro-nano structure of the PANI electrode can be the main reason for pH sensor capability because of its potential stability to facilitate redox reactions. SEBS substrate could be stretched to 100% (Fig. 2C), and microcracks were present on gold layer by SEM imaging (Fig. 2D). This morphology is formed spontaneously under specific parameters. The gold electrode can be stretched by this kind of microcrack. The microcracked gold film can share the stress under tension by crack expansion, that is, in the tensile process, although the crack area of the gold electrode expands, there is always a part to maintain the connection. In this way, the extensibility of the electrode is realized.[16] The stretchability was further confirmed by the sustained conductivity when the tensile resistance exceeds 100% (Fig. 2E).

The flexible materials used in wound monitoring was compared in Table S1 and Fig. S1.† Previous studies focused on demonstrating the function of the device, however, the softness of the material itself and the adhesion of the wound are also important.[24,30,31] The conformability of these materials were not satisfactory. Flexural stiffness (D) of the sensor is defined as: $D = Eh^3/12\ (1 - \nu^2)$, where E is the elastic modulus, h is the thickness of the sensor and ν is Poisson's ratio. Higher E or h will lead lager D, resulting in a poor conformability for the devices. For the reported typical dressings, the flexural stiffness is too high to conform on skin, and need to be further improved to adhere better to the skin.[35] The stretchable property of the SEBS substrate also facilitates its application on the skin of joints.[36,37] Comparison with a non-stretchable PI substrate on the finger joint shows that the SEBS film can deform to fit maximum movements of the finger joint to 105°, which is close to the maximum angle of a finger bend. By contrast, non-stretchable PI film can only rely on the stretchability of the skin for finger joint bends of 45°, due to the ductility of human skin (Fig. 2G and H). This result suggested that stretchability is important for the application of flexible materials in wearable devices.

3.2. Sensing performance of the pH sensor

The measurement of the OCP between the PANI sensing electrode and Ag/AgCl reference electrode provided electrochemical characteristics of the pH sensor. Fig. 3A shows a schematic diagram of the sensor electrochemical test. Both the work and reference electrodes were immersed in different pH buffers to obtain different OCPs.

The stability of pH sensor was investigated under 300 cycles of tension as shown in Fig. S3,† the corresponding SEM image is shown in Fig. S4.† After 300 times of 50% stretching, the potential changes slightly, and the error of pH is less than 0.07 (Fig. 3B). The micro morphology of the sensor after stretching has not changed greatly, due to the recovery of microstructure, the performance of the sensor also changes little. This property insured its application in an actual wound. The OCP signals of the pH sensor were studied at different pH values in the range of 4–10, and the stability was explored (Fig. 3C). PANI undergoes protonation or deprotonation reaction in acidic or alkaline solution to present different OCP value.[24,32] The OCP signal showed a linear relationship with the pH value, and the

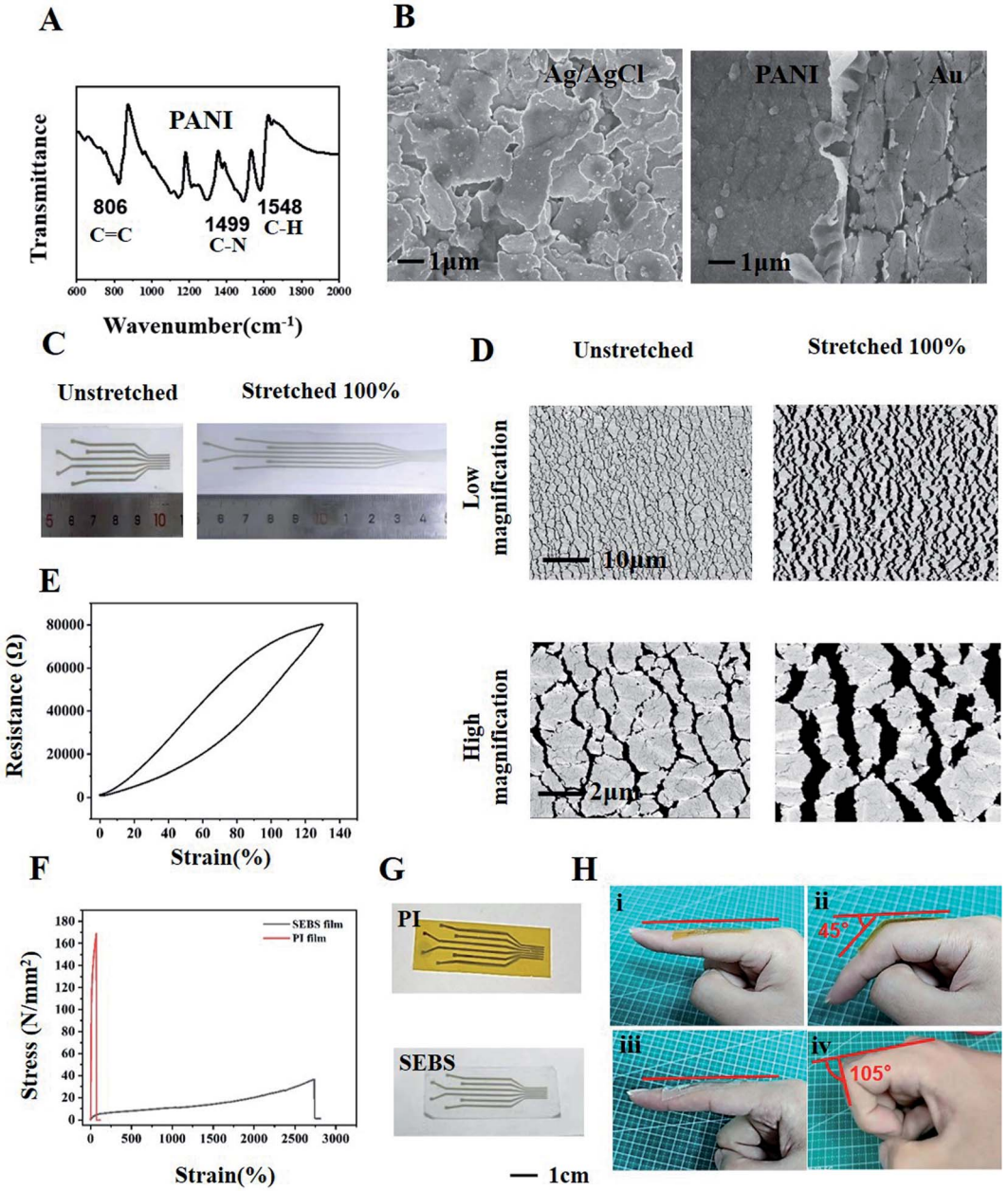

Fig. 2 Structure characterization and flexible characterization of pH sensor. (A) Infrared spectrum of Polyaniline, (B) SEM of cured Ag/AgCl ink and the boundary between polyaniline and gold, (C) unstretched and stretched 100% SEBS substrate with gold layer, (D) SEM of unstretched and stretched 100% SEBS substrate with gold layer, (E) Stress-resistance curves of SEBS substrate with gold layer, (F) stress–strain curves of two substrates, (G) gold layer on PI film and SEBS film, (H) stretching comparison between PI film (I and II) and SEBS film (III and IV) on finger joint.

standard calibration line of the pH sensor was obtained by linear fitting (Fig. 3D). The sensitivity of the potentiometric pH sensor can be obtained by the slope of the linear regression, according to the Nernst equation: $E = E^0 - (2.303RT/F)\,\mathrm{pH} = E^0 - 0.05916\,\mathrm{pH}$, where R is the gas constant, T is the temperature, E^0 is the standard electrode potential, and F is Faraday's constant. Based on Nernst behavior, the theoretical maximum sensitivity is -59 mV pH^{-1} at room temperature. The resultant calibration curve is linear, with a slope of -65.9 mV pH^{-1} ($R^2 = 99.8\%$) in a wide pH range of pH 4–10. This sensitivity value of the pH sensor is close to the theoretical pH sensitivity based on Nernstian behavior and is similar to other previous reports based on PANI electrodes. And we compared it with other similar studies, and the results are shown in Table S2.† The pH of normal skin is weakly acidic, and the pH of the wound is neutral due to the exposure of plasma. When infection occurs, the pH will raise to alkaline, ranging between 7 and 9.[25] These results indicate that the pH sensor could cover the range of pH changes in different stages of the wound, and it was well matched with the theoretical accuracy.

The response time of the pH sensor was measured by increasing the pH (Fig. 3E). The OCP signal was subsequently

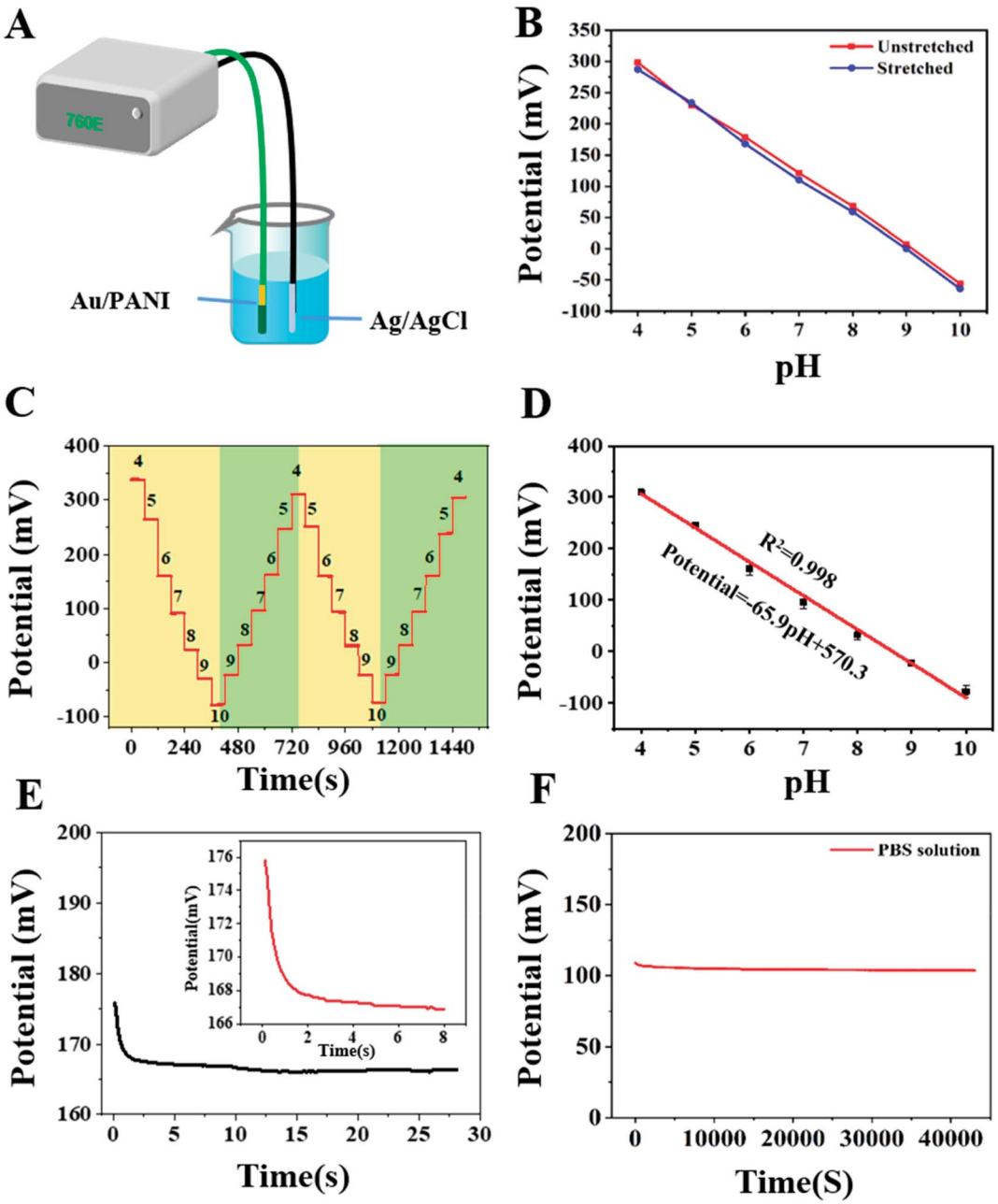

Fig. 3 Electrochemical investigation of the fabricated pH sensor. (A) Schematic diagram of sensor electrochemical test, (B) potential test under tensile condition, (C) potential calibration in the pH range of 4 to 10, (D) fitting calibration chart of sensor, (E) response time of pH sensor form pH6 to pH 6.25, (F) stability test of pH sensor in PBS (pH 7.2).

changed and reached 90% of its steady state value within 6 s. The improvement in the response time depends on the uniformity of the microstructure; the uniform distribution of polyaniline makes the response instant and rapid. The fast response time of the pH sensor indicates that this sensor can be applied in situations where dynamic pH changes occur.

The long-term stability of the pH sensor was further studied by measuring the OCP response of the pH sensor after immersing in PBS for 12 hours (Fig. 3F). The pH sensor maintained the OCP signals, resulting in a potential drift within 2.0 mV h^{-1}, which corresponds to a 0.036 error in the pH value after an hour of continuous measurement. The stability of the pH sensor could still be guaranteed even after a long-term measurement-a feature that is very important in the actual application of wound monitoring, and this sensor met this requirement. Modification of the gold electrode allowed successful preparation of the pH sensor on flexible stretchable substrate, and the sensor showed good sensitivity and stability.

3.3. Sensing performance of the temperature sensor

The temperature sensor was fabricated based on a commercial TMP112 chip. Its structure diagram is shown in Fig. 4A. The

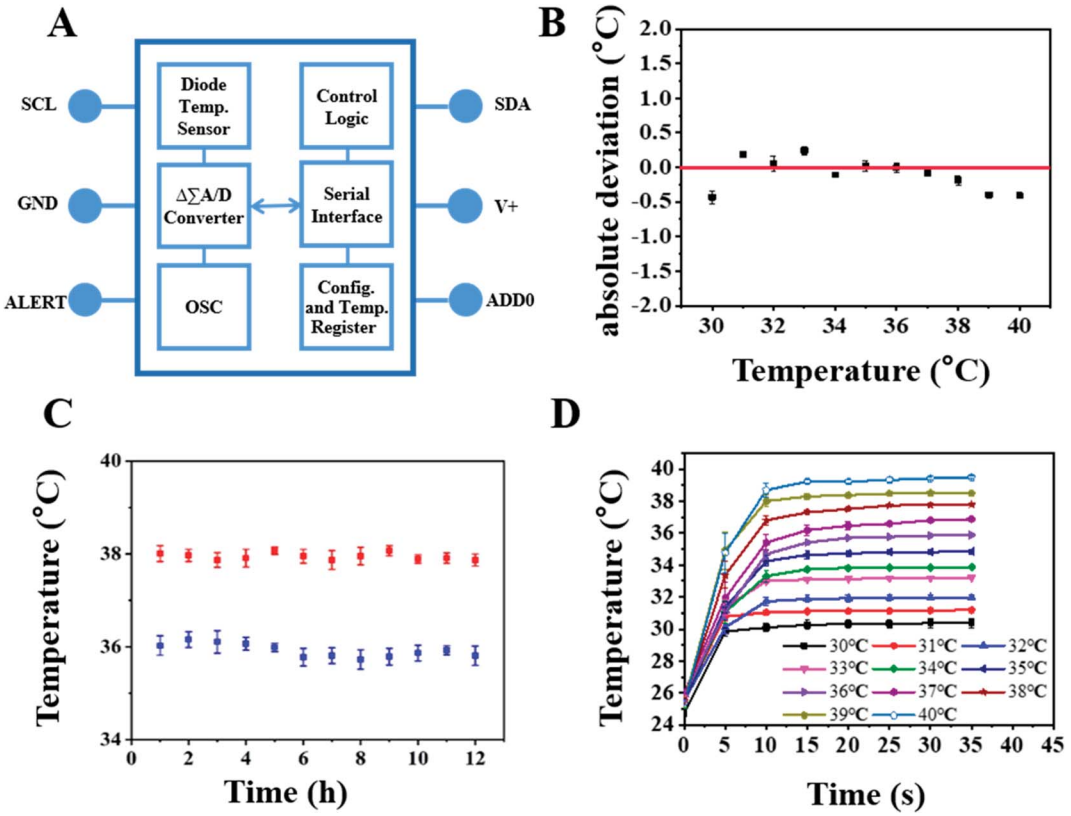

Fig. 4 Performance test of temperature sensor. (A) Structure diagram of temperature sensor circuit connection, (B) sensitivity test of temperature sensor, (C) stability test of temperature sensor, (D) response time test of temperature sensor.

commercial temperature sensor (TMP112AIDRLR) was chosen because it featured high precision, low power consumption, and a small volume size that satisfied our temperature monitoring needs for wounds. In previous studies, this type of chip has been used in biological and physical health monitoring.[19]

The accuracy, responsiveness, and durability of the PDMS-encapsulated commercial temperature sensor were checked by first placing the sensor inside a Ziplock bag before inserting it into a temperature-controlled water bath with a temperature ranging from 30 to 40 °C, which covers body temperature range. The mean displayed temperature values recorded after 1 min of monitoring indicated that the temperature sensor had excellent accuracy, with an absolute deviation of < ±0.4 °C (Fig. 4B). Fig. 4C shows that the chip has good stability, which is necessary for real-time monitoring. As shown by the temperature–time curve (Fig. 4D), the temperature sensor displayed a response time of < 30 s and long stability. The performance of the TMP112A temperature sensor could therefore satisfy the needs of real-time and *in situ* wounding monitoring. Coupling of this sensor with the SEBS substrate Au-PANI pH sensors in a specific geometric distribution would therefore allow simultaneous monitoring of the wound pH and temperature. In summary, a commercial temperature sensor with a small volume and high sensitivity was selected and integrated onto an FPCB by a simple circuit connection.

3.4. Biocompatibility of the device and monitoring of infection in cutaneous wounds

Good biocompatibility is essential for the materials used in a wound dressing to ensure that the dressing will not cause damage to the wound bed when in contact with the wound surface. The toxicity of the materials used in the sensor was evaluated by the viability of L929 cells exposed to the material extracts utilized in the sensor. The results from the quantitative CCK-8 assay showed that the SEBS and pH sensor extracts were noncytotoxic, as the relative cell viability was greater than 95% (Fig. 5A). These results confirmed that the materials used in the sensor were biocompatible.

The flexible detection system was verified *in vitro* to monitor the changes in pH and temperature, and its performance in actual wound monitoring was then investigated. The rat model of infection was established by inoculating *S. aureus* into cutaneous wounds. *S. aureus* is one of the most common bacterial pathogens found in infected wounds.[38,39] The rats were divided into two groups: infected and uninfected. Photographs of the wounds at 0, 8, 24, 32, 54, and 78 h are shown in Fig. 5B. Purulent discharge was clearly visible in the infected group on the third day, accompanied by wound redness and swelling, indicating that the infection had induced inflammation and tissue necrosis.[39,40] H&E staining of the skin biopsies of the wound sites showed inflammation infiltration in the infected group (Fig. 5C). At 8 and 30 h after inoculation, many more

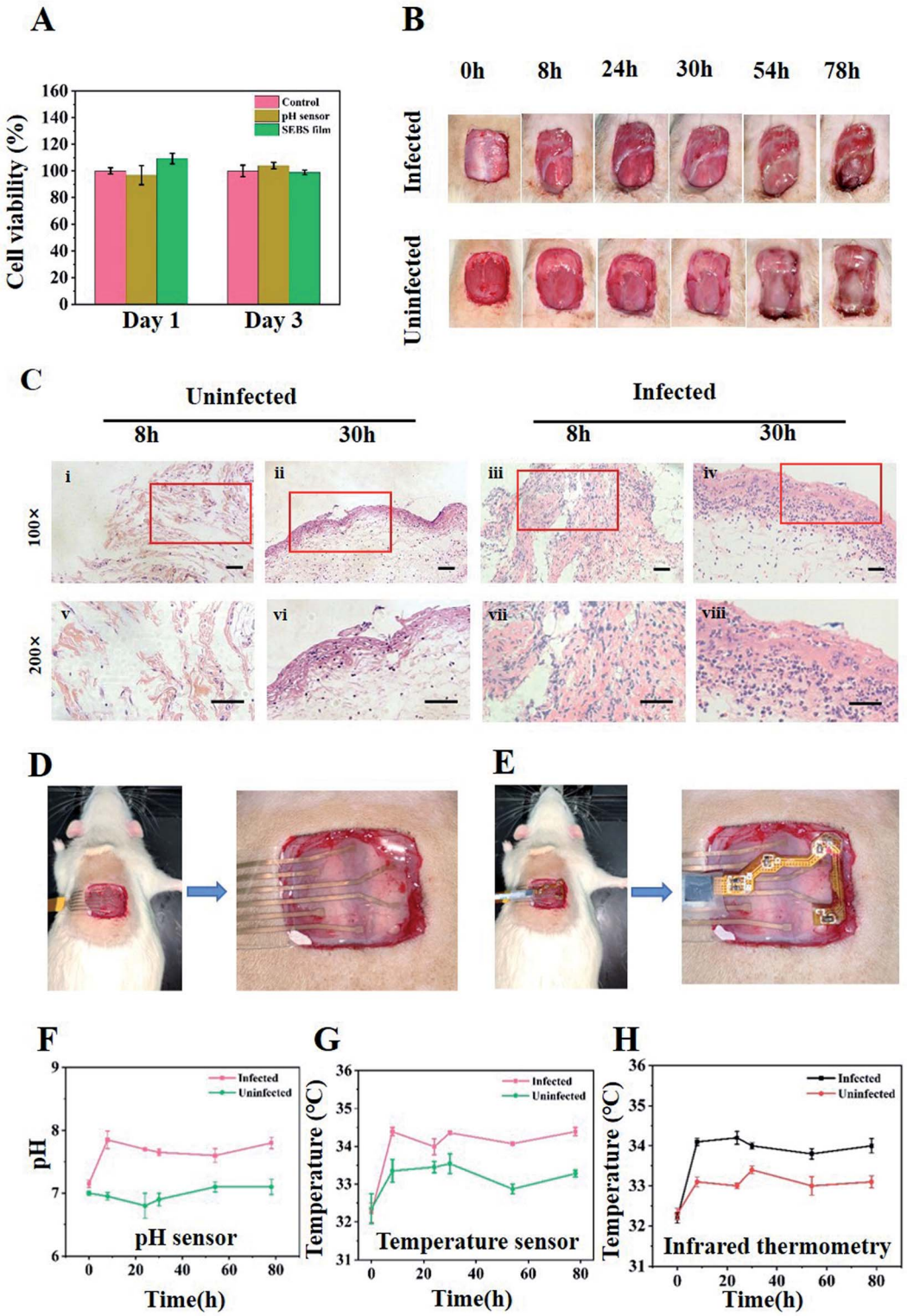

Fig. 5 Biocompatibility of the device and monitoring of infection in cutaneous wounds. (A) Cell viability test of pH sensors. (B) Photographs of *S. aureus* infected wounds in rat. Changes of infected and uninfected wounds, (C) observe the tissue section of the uninfected wound under a low power microscope for 8 h (I) and 30 h (II), tissue section of infected wound for 8 h (III) and 30 h (IV), observe the tissue section of the uninfected wound under a high-power microscope for 8 h (V) and 30 h (VI), Tissue section of infected wound for 8 h (VII) and 30 h (VIII). (D) and (E) Physical image of sensor for wound monitoring, (F) pH changes of wound, (G) temperature change of wound, (H) temperature change measured by infrared thermometer.

immune cells had accumulated in the cutaneous wounds in the infected group than in the uninfected group. Neutrophils could usually be found in *S. aureus* infected wounds as innate immune cells in the early inflammatory response.[39,41] These results demonstrated the establishment of an infected wound.

The image of the sensor attached to the wound shows that the flexible dressing fit well with the wound (Fig. 5D and E) and was able to monitor the changes in pH (Fig. 5F) and temperature (Fig. 5G) in the wound. The infection induced a rise in pH and temperature at the wound sites as early as 8 h post operation. When the wound was just created, it had a pH around 7–7.2 and a body surface temperature of about 32.4 °C. Eight hours later, the pH of the infected wound had increased to pH 7.7 and the temperature had risen to 34.1 °C. A comparison of infrared thermometers revealed close results (Fig. 5H). By contrast, the pH and temperature of the uninfected wound surface increased only slightly. In the following 3 days, although the pH and temperature of the two wound surfaces fluctuated, the pH and temperature were always higher for the infected wound than for the uninfected one, due to the proliferation of bacteria and the response of the rat's own immune system.[28] In the animal model experiment, the customized data processing module is integrated with the sensor for data acquisition. Due to the limitations of the size and energy of the data processing module, continuous wound monitoring was not performed in this study. However, with the development of smaller back-end modules and the further optimization of sensor materials, long-term real-time monitoring of wounds will be possible.

As mentioned earlier, the pH value of the wound is an important biomarker that can provide important information about the condition of the wound. The pH of the surface of normal skin is acidic, but injury can lead to the exposure of the underlying tissue and change the acidic environment of the site. When infection occurs, the changes caused by bacterial metabolism and proliferation will make the pH of wound reach alkaline state.[42] Other articles have mentioned temperature as a parameter influenced by many factors, such as blood flow, bacterial infection, and oxygenation. Inflammation, new tissue formation, and remodeling during wound healing can also raise the temperature.[19,43] In this system, the temperature chip was integrated on the FPCB, since the combination of hard chip and soft substrate is difficult to realize, however, this should be worked on in the future. Comparison of with the changes in pH and temperature confirmed that the sensor fabricated here can detect these changes at the corresponding time; that is, the change can be used as an early warning that the wound is infected.[44] In clinic, the wounds usually are more complex, and many factors wound influence the result, such at body fluid, ambient temperature. In addition, the combination of hard chip and soft substrate is a future attempt.

4. Conclusion

In this work, we have successfully developed a soft wound infection monitoring system consisting of a pH sensor and a temperature sensor. We used a soft enough substrate so that the dressing can be well applied to the wound skin, and sensors with arrays make monitoring more accurate. The pH sensor is integrated on a soft and stretchable substrate and shows good sensitivity, linearity, biocompatibility, and wearability in contact with wounds. The temperature sensor chip is attached to the pH sensor and integrated onto the FPCB. Through a series of *in vitro* tests and the establishment of infection models, the soft system confirmed its reliable performance and good conformity with the skin. The applicability of the system was verified by *in vitro* characterization and *in vivo* model testing. This study provides a soft wearable monitoring system for real-time monitoring of wound infection.

Author contributions

Conceptualization: Xiaoli Zhao. Resources: Zhiyuan Liu. Data curation: Zhiyang Zhang, Rui Su, Fei Han. Software: Xiaomeng Zhou. Formal Analysis: Zhiqiang Zheng, Yuan Liu. Supervision: Peizhi Guo, Zhaoyang Li. Funding acquisition: Xiaoli Zhao. Validation: Jun Wu, Xiaohua Pan, Xinyun Zhai. Project administration: Haobo Pan. Writing – original draft: Zhiyang Zhang, Rui Su, Fei Han. Writing – review & editing: Qingsong Li.

Conflicts of interest

The authors declare that they have no known competing financial interests or personal relationships that could have appeared to influence the work reported in this paper.

Acknowledgements

This work was supported by the National Key R&D Program of China (2018YFA0703100), Science and Technology Research Funding of Shenzhen (JSGG20180503182359108, JCYJ20200109150420892), and Major Scientific and Technological Innovation Projects of Shandong Province (2019JZZY011112).

References

1 H. S. Kim, X. Sun, J. H. Lee, H. W. Kim, X. Fu and K. W. Leong, *Adv. Drug Delivery Rev.*, 2019, **146**, 209–239.
2 E. M. Tottoli, R. Dorati, I. Genta, E. Chiesa, S. Pisani and B. Conti, *Pharmaceutics*, 2020, **12**, 735–740.
3 L. J. Bessa, P. Fazii, M. Di Giulio and L. Cellini, *Int. Wound J.*, 2015, **12**, 47–52.
4 I. Dietrich, G. A. Braga, F. G. de Melo and A. C. C. da Costa Silva Silva, *Curr. Atheroscler. Rep.*, 2017, **19**, 44–48.
5 K. Rahim, S. Saleha, X. Zhu, L. Huo, A. Basit and O. L. Franco, *Microb. Ecol.*, 2017, **73**, 710–721.
6 K. Ottolino-Perry, E. Chamma, K. M. Blackmore, L. Lindvere-Teene, D. Starr and K. Tapang, *Int. Wound J.*, 2017, **14**, 833–841.
7 P. Mostafalu, A. Tamayol, R. Rahimi, M. Ochoa, A. Khalilpour and G. Kiaee, *Small*, 2018, e1703509.
8 J. G. Powers, C. Higham, K. Broussard and T. J. Phillips, *J. Am. Acad. Dermatol.*, 2016, **74**, 607–625.

9 S. Schreml, R. M. Szeimies, S. Karrer, J. Heinlin, M. Landthaler and P. Babilas, *J. Eur. Acad. Dermatol. Venereol.*, 2010, **24**, 373–378.
10 H. J. Park, J. H. Yoon, K. G. Lee and B. G. Choi, *Nano Convergence*, 2019, **6**, 9–15.
11 Y. S. Kim, M. Mahmood, Y. Lee, N. K. Kim, S. Kwon and R. Herbert, *Adv. Sci.*, 2019, **6**, 1900939.
12 K. Y. Kwon, Y. J. Shin, J. H. Shin, C. Jeong, Y. H. Jung and B. Park, *Adv. Healthcare Mater.*, 2019, **8**, e1801593.
13 M. Caldara, C. Colleoni and E. Guido, *IEEE*, 2013, 1–6.
14 M. Gong, P. Wan, D. Ma, M. Zhong, M. Liao and J. Ye, *Adv. Funct. Mater.*, 2019, **29**, 1902127.
15 W. Gao, H. Ota, D. Kiriya, K. Takei and A. Javey, *Acc. Chem. Res.*, 2019, **52**, 523–533.
16 N. Matsuhisa, Y. Jiang, Z. Liu, G. Chen, C. Wan and Y. Kim, *Adv. Electron. Mater.*, 2019, **5**, 1900347.
17 G. K. Mani, Y. Nimura and K. Tsuchiya, *ACS. Sens.*, 2020, **5**, 911–916.
18 L. Xu, S. R. Gutbrod, A. P. Bonifas, Y. Su, M. S. Sulkin and N. Lu, *Nat. Commun.*, 2014, **5**, 3329–3337.
19 Q. Pang, D. Lou, S. Li, G. Wang, B. Qiao and S. Dong, *Adv. Sci.*, 2020, **7**, 1902673.
20 Y. Yang and W. Gao, *Chem. Soc. Rev.*, 2019, **48**, 1465–1491.
21 R. Rahimi, U. Brener, S. Chittiboyina, T. Soleimani, D. A. Detwiler and S. A. Lelièvre, *Sens. Actuators, B*, 2018, **267**, 198–207.
22 M. Sharifuzzaman, A. Chhetry, M. A. Zahed, S. H. Yoon, C. I. Park and S. Zhang, *Biosens. Bioelectron.*, 2020, **169**, 112637.
23 A. Tamayol, M. Akbari, Y. Zilberman, M. Comotto, E. Lesha and L. Serex, *Adv. Healthcare Mater.*, 2016, **5**, 711–719.
24 R. Rahimi, M. Ochoa, T. Parupudi, X. Zhao, I. K. Yazdi and M. R. Dokmeci, *Sens. Actuators, B*, 2016, **229**, 609–617.
25 L. A. Schneider, A. Korber, S. Grabbe and J. Dissemond, *Arch. Dermatol. Res.*, 2007, **298**, 413–420.
26 Y. Yao, J. Chen, Y. Guo, T. Lv, Z. Chen and N. Li, *Biosens. Bioelectron.*, 2021, **179**, 113078.
27 M. A. Zahed, S. C. Barman, P. S. Das, M. Sharifuzzaman, H. S. Yoon and S. H. Yoon, *Biosens. Bioelectron.*, 2020, **160**, 112220.
28 Y. Kim, C. Park, S. Im and J. H. Kim, *Sci. Rep.*, 2020, **10**, 16488.
29 X. Chen, L. Yin, J. Lv, A. J. Gross, M. Le and N. G. Gutierrez, *Adv. Funct. Mater.*, 2019, **29**, 1905785.
30 G. Xu, Y. Lu, C. Cheng, X. Li, J. Xu and Z. Liu, *Adv. Funct. Mater.*, 2021, **29**, 1902127.
31 S. P. Lacour, G. Courtine and J. Guck, *Nat. Rev. Mater.*, 2016, **1**, 16063.
32 Y. Li, Y. Mao, C. Xiao, X. Xu and X. Li, *RSC Adv.*, 2020, **10**, 21–28.
33 A. J. Bandodkar, V. W. Hung, W. Jia, G. Valdes-Ramirez, J. R. Windmiller and A. G. Martinez, *Analyst*, 2013, **138**, 123–128.
34 T. Guinovart, G. A. Crespo, F. X. Rius and F. J. Andrade, *Anal. Chim. Acta*, 2014, **821**, 72–80.
35 J. R. Sempionatto, M. Lin, L. Yin, E. De la Paz, K. Pei and T. Sonsa-Ard, *Nat. Biomed. Eng.*, 2021, **5**, 737–748.
36 K. Zhou, K. Dai, C. Liu and C. Shen, *SmartMat*, 2020, **1**, e1010.
37 X. Chen, L. Yin, J. Lv, A. J. Gross, M. Le and N. G. Gutierrez, *Adv. Funct. Mater.*, 2019, **29**, 1905785.
38 J. Li, X. M. Liu, L. Tan, Z. D. Cui, X. J. Yang and Y. Q. Liang, *Nat. Commun.*, 2019, **10**, 4490–4504.
39 W.-T. Yang, C.-Y. Ke, W.-T. Wu, Y.-H. Tseng and R.-P. Lee, *Sci. Rep.*, 2020, **10**, 5596.
40 R. P. Adhikari, C. D. Thompson, M. J. Aman and J. C. Lee, *Vaccine*, 2016, **34**, 6402–6407.
41 R. V. Ortines, H. Liu, L. I. Cheng, T. S. Cohen, H. Lawlor and A. Gami, *Antimicrob. Agents Chemother.*, 2018, **62**, e02288.
42 Y. Hattori, L. Falgout, W. Lee, S. Y. Jung, E. Poon and J. W. Lee, *Adv. Healthcare Mater.*, 2014, **3**, 1597–1607.
43 H. Derakhshandeh, S. S. Kashaf, F. Aghabaglou, I. O. Ghanavati and A. Tamayol, *Trends Biotechnol.*, 2018, **36**, 1259–1274.
44 S. L. Swisher, M. C. Lin, A. Liao, E. J. Leeflang, Y. Khan and F. J. Pavinatto, *Nat. Commun.*, 2015, **6**, 6575–6585.